Crossed-Beam Energy Transfer in Inertial Confinement Fusion Implosions on OMEGA

Inertial confinement fusion (ICF) uses the energy of multiple laser beams to implode a millimeter-scale capsule containing nuclear fuel.[1] Direct-drive implosions are driven by heat that is generated by the absorption of laser light ($I \sim 10^{14}$ to 10^{15} W/cm^2) in a plasma corona surrounding the capsule.[2] The crossed-beam energy transfer (CBET) caused by stimulated Brillouin scattering (SBS)[3] reduces the laser absorption, making it possible for incoming light to bypass the highest absorption region near the critical radius, at which the electron number density n_e equals the critical density $n_{cr} = \pi c^2 m_e / \lambda_L^2 e^2$, where λ_L is the laser wavelength in vacuum. Under certain conditions, the CBET may be large and significantly reduce the performance of ICF implosions.[4–6]

In this article, the effect of SBS in implosion experiments on the OMEGA Laser System,[7] operating at $\lambda_L = 351$ nm, is investigated. The results of a new CBET model coupled to the one-dimensional radiative hydrodynamic code *LILAC*[8] are presented and quantitatively compared with experimental results. It is shown that the best agreement between simulations and scattered-light[9] and bang-time[10] measurements can be obtained by simultaneously employing the CBET and non-local thermal transport.[11,12] *LILAC* simulations show that using two-color laser light with a wavelength separation $\Delta\lambda \sim 5$ to 8 Å can reduce the CBET and increase the absorption, thereby improving the implosion efficiency.

The CBET model considers the propagation of two crossing laser beams (probe and pump) in a moving plasma and the interaction of these beams with an ion-acoustic wave (IAW) that they excite.[4,13,14] Assuming s-polarized light and steady state, the probe beam intensity $I^{(1)}$ along the path ℓ can be calculated as follows:

$$I^{(1)} = I_0^{(1)} \exp \left\{ \int \left[\eta L_{CBET}^{-1} - L_{IB}^{-1} \right] d\ell \right\}, \qquad (1)$$

where L_{IB} is the inverse bremsstrahlung absorption scale length,[3] L_{CBET} is the scale length of energy loss or gain caused by CBET, and η is an adjustment parameter $0 \le \eta \le 1$. The scale length L_{CBET} is defined by

$$L_{CBET}^{-1} = 0.0585 \frac{n_e / n_{cr}}{\sqrt{1 - n_e / n_{cr}}}$$

$$\times \frac{\lambda_{L,\mu m} I_{14}^{(2)}}{\left(1 + 3 T_i / Z T_e\right) T_{e,keV}} \frac{P(\chi)}{\tilde{\nu}_a} \mu m^{-1}, \qquad (2)$$

where $\lambda_{L,\mu m}$ is the laser wavelength in microns, $I_{14}^{(2)}$ is the pump-beam intensity in units of 10^{14} W/cm^2, T_e and T_i are the electron and ion temperatures ($T_{e,keV}$ in keV), Z is the average ionization, ν_a is the damping coefficient for IAW's, $\tilde{\nu}_a = \nu_a / k_a c_a$ is the dimensionless damping,

$$P(\chi) = \frac{\tilde{\nu}_a^2 \chi}{\tilde{\nu}_a^2 \chi^2 - \left(1 - \chi^2\right)} \qquad (3)$$

is the resonance function,[4] $\chi = -\omega_a / k_a c_a + (\mathbf{k}_a \cdot \mathbf{u}) / k_a c_a$, $\mathbf{u}$ is the velocity vector, c_a is the ion-acoustic velocity, $\omega_a = \omega_1 - \omega_2$ and $\mathbf{k}_a = \mathbf{k}_1 - \mathbf{k}_2$ are the IAW frequency and wave vector, respectively, and ω and $\mathbf{k}$ with the lower indexes 1 and 2 are the frequencies and wave vectors of the probe and pump light, respectively.

The CBET model has been incorporated into the laser absorption algorithm in *LILAC*. The algorithm calculates the integral in Eq. (1) along various light-ray paths, accounting for all possible beam crossings in three dimensions. Doppler shift of the light frequencies is calculated using the equation $\Delta\omega = \omega_L (\partial\tau / \partial t)$ (Ref. 15), where τ is the light-wave flight time and $\omega_L = 2\pi c / \lambda_L$. The damping is approximately $\tilde{\nu}_a \approx 0.2$ for CH plasma under the considered conditions.[16] Simulations, however, showed a weak dependence on $\tilde{\nu}_a$ over the interval $0.1 < \tilde{\nu}_a < 0.5$.

The energy is not conserved exactly in Eq. (1) because pump-light depletion is neglected. To enforce this conservation, the algorithm normalizes the total energy gain (or loss) for outgoing light to the total energy loss (or gain) for incoming

light at each radius. Calculations were significantly simplified assuming a uniform illumination of implosion capsules (but the intensity profile inside the beams is retained). Test simulations using this simplified assumption and the illumination by all 60 OMEGA beams showed good agreement between the two approaches. The random polarization of light on OMEGA is accounted for by reducing the numerical factor in Eq. (2) by 0.5.

Typical implosion targets on OMEGA are room-temperature-D_2- or DT-gas–filled plastic shells and cryogenic D_2- or DT-ice shells with a thin plastic overcoat. The outer diameter is about 840 to 880 μm. Laser pulses can have various shapes with pickets and pedestals, have durations from 0.1 to 4 ns, and deliver on target up to 30 kJ. *LILAC* simulations of OMEGA implosions have revealed the importance of CBET at laser intensities $I \gtrsim 10^{14}$ W/cm^2. At $I > 5 \times 10^{14}$ W/cm^2, the energy transfer can reach a significant level $\gtrsim$30% of the incident energy. The CBET is most efficient in a radially extended plasma corona, which develops after the first 100 to 200 ps of a pulse. The transfer occurs in a relatively wide radial interval ~50 μm, in which n_e is in the range of 0.2 to 0.3 n_{cr} (see Fig. 122.14). As a result, the absorption is spatially redistributed, shifting outward, and its integrated value can be changed [see black and blue lines in Fig. 122.14(a)]. The most-energetic transfers involve the incoming light with small impact parameters (at the beam center) and outgoing light, which is inclined at ~20° to 30° with respect to the radial direction. The former light

looses some energy and the latter gains the energy. The nonzero angles between interacting light rays explain our finding that the energy transfer is maximized at the supersonic region of the corona, at $u_r/c_a \approx 1.4$ [see the red line in Fig. 122.14(a) and the blue dashed line in Fig. 122.14(b)], instead of at the transonic point, $u_r/c_a = 1$, if the angles were close to zero.[5] Here, u_r is the radial component of the velocity. Fortunately, most CBET interaction occurs at moderate angles ($\lesssim$25°), where the paraxial approximation used in Eq. (2) is valid.

The CBET redistributes the energy inside the laser beams from light rays with small impact parameters to light rays with larger ones. This redistribution and corresponding modification of the absorption can be emulated using the effective profile in which the beam's central intensity is decreased and the beam's edge intensity is increased (see Fig. 122.15). Such effective profiles may be useful in multidimensional simulations in which the direct employment of the CBET model is highly impractical.[17]
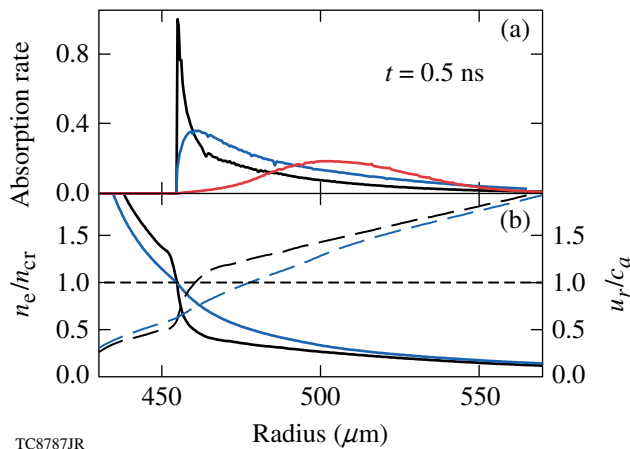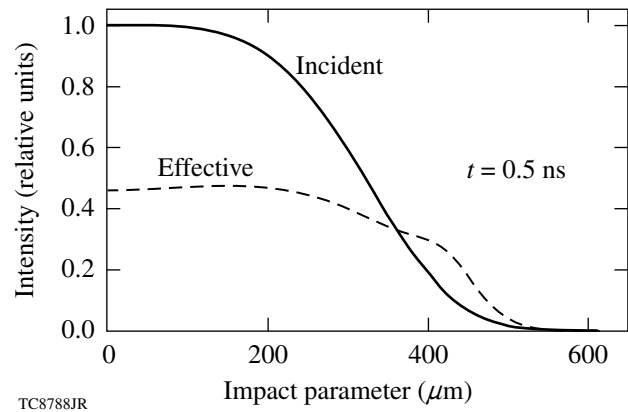

TC8788JR

Figure 122.15
Incident (super-Gaussian with an index $n = 4$) and effective beam profiles at $t = 0.5$ ns for the same simulation with nonlocal transport and CBET as shown in Fig. 122.14. The effective profile emulates the loss ($\approx$26%) and redistribution of the energy inside the beam caused by CBET.

TC8787JR

Figure 122.14
Simulated (a) absorption rate per unit volume (in relative units, black and blue lines) and (b) relative electron density n_e/n_{cr} (solid lines) and Mach number u_r/c_a (dashed lines), at $t = 0.5$ ns for an 880-μm-diam plastic shell (20-μm CH wall) imploded with a 1-ns square pulse at $I \sim 10^{15}$ W/cm^2. The simulations with flux-limited transport ($f = 0.06$) are shown in black and nonlocal transport and CBET ($\eta = 0.75$) in blue. The CBET rate (in relative units) from incoming to outgoing light is shown in (a) in red.

OMEGA planar and implosion experiments are typically simulated by employing the Spitzer thermal transport[18] with flux limitation, in which the phenomenological constant-value flux-limiting parameter f is used.[19] Assuming $f = 0.06$, the model can explain reasonably well planar shock-timing experiments[20] and implosion experiments with short ($\lesssim$1 ns), square pulses.[11] In the case of long, shaped pulses, however, the flux-limited transport experiences difficulties in consistently explaining the whole range of experimental data, including

bang-time and scattered-light measurements.[11] The inaccuracy of the flux-limited transport becomes especially apparent in adiabat-shaped designs[21,22] in which a time-dependent flux limiting was proposed.[11,23]

A step-up from the Spitzer transport is the nonlocal transport model,[11,12] which calculates heat fluxes by solving the simplified Boltzmann equation and employing the Krook approximation.[24] This transport introduces two major improvements. First, the flux in regions with steep temperature gradients is reduced from the Spitzer value, eliminating the need for flux limitation. Second, the heating by long-range hot electrons is accounted for. The latter introduces changes in the density scale length near n_{cr}, making this length longer by a factor of ~10 [Fig. 122.14(b)]. The longer scale length significantly reduces the prediction for resonance absorption[25] and reduces the strong bremsstrahlung absorption peak near critical density [Fig. 122.14(a)]. Simulations using the nonlocal transport predict well the shock-timing experiments with short picket pulses (~100 to 200 ps), but they over-predict the laser drive in implosions with long pulses.[9]

The agreement between simulations and experiments is significantly improved when the nonlocal transport and CBET are used simultaneously. As an example, Fig. 122.16 compares

the measurement and various simulations of time-resolved scattered-light power for a plastic-shell implosion (OMEGA shot 56830). The simulated power, using nonlocal transport and CBET (green line), shows very good agreement with the scattered-light measured power (thick black line) for $\eta = 0.75$. The models without CBET, which use flux-limited or nonlocal transport (red and blue lines, respectively), clearly underestimate the scattered power. Similar results were found in simulations of different warm and cryogenic implosions.

Figure 122.17 shows the neutron-production history for the implosion in Fig. 122.16. Again, the bang time inferred from the neutron data predicted in the model with CBET (thin solid line) shows very good agreement with the bang time inferred from the measured neutron data (thick solid line). In contrast, the bang times inferred from the results of the models without CBET (dashed and dotted lines in Fig. 122.17) are about 150 ps earlier. The reduction of the measured neutron rate with respect to the predicted rates in Fig. 122.17 is due to the growth of perturbations from laser imprint, which affects the implosion performance[1] and is not considered in *LILAC* simulations.

Based on simulations of warm and cryogenic implosions with different laser energies and pulses, one concludes that bang-time and scattered-light measurements can typically
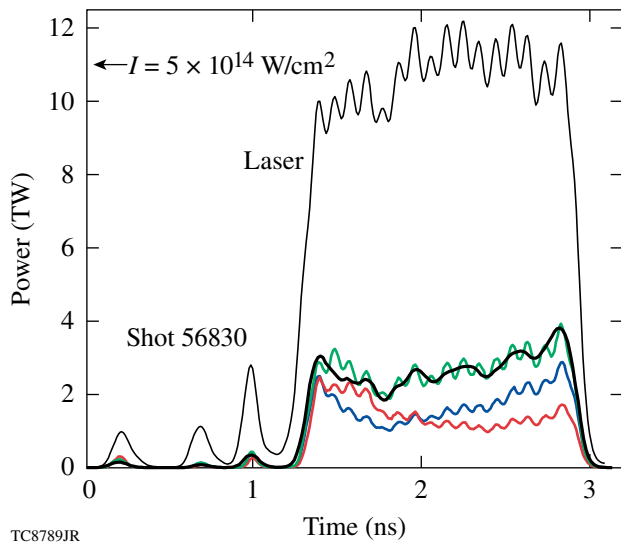
Figure 122.16

Scattered-light power for an 830-μm-diam plastic shell (9 atm of D_2-gas fill, 26-μm CH wall) imploded with 18.3 kJ. The incident laser power and experimental scattered power (within ±5% accuracy) are shown by the thin and thick black lines, respectively. The *LILAC* predictions with flux-limited ($f = 0.06$) and nonlocal transports are shown in red and blue, respectively, and with nonlocal transport and CBET ($\eta = 0.75$) in green.
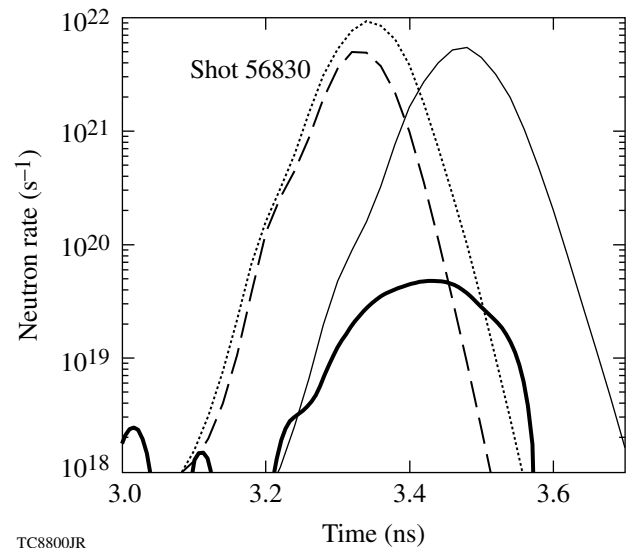
Figure 122.17

Neutron-production history for the same implosion as in Fig. 122.16. The measured history (thick solid line) is determined with ~50-ps uncertainty. The *LILAC* predictions with flux-limited ($f = 0.06$) and nonlocal transports are shown by the dashed and dotted lines, respectively, and with nonlocal transport and CBET ($\eta = 0.75$) by the thin solid line.

be explained using a somewhat-reduced CBET, in which η is assumed between 0.5 and 1. This relatively wide uncertainty interval of η can be partially attributed to the uncertainties of experimental results. It is apparent, however, that the experimentally suggested mean value $\eta \sim 0.75$ is smaller than the theoretical prediction $\eta = 1$. This suggests the inaccuracy of the simplified CBET model [Eqs. (1)–(3)] is of the order of ~25%.

Since the light refraction and frequency shift are sensitive to the corona's spatial structure, the simulated coronal structure can be validated using time-dependent scattered-light spectral measurements.[9] Figure 122.18 shows an example of the measurement and simulations for an 843-μm-diam plastic shell (20-μm CH wall) imploded with 1-ns square pulse at $I \sim 8 \times 10^{14}$ W/cm^2 (OMEGA shot 50601). Two simulations are compared using (1) flux-limited transport [Fig. 122.18(b)] and (2) nonlocal transport and CBET [Fig. 122.18(c)]. Both simulated spectra reproduce reasonably well the basic structure of the measured spectrum [Fig. 122.18(a)]. The initial (at $t \lesssim 0.5$ ns) blue shift is attributed to the Doppler shift of light reflected in the expanding part of the corona and the late-time (at $t \gtrsim 0.5$ ns) red-shifted "fan tails" are produced by light reflected in the inward-moving part. However, these simulations reveal important differences. The flux-limited model predicts an insufficient initial blue shift [Ref. 26, feature A in Fig. 122.18(b)], which clearly deviates from the measured spectrum. The blue shift predicted by the model with nonlocal transport [Fig. 122.18(c)] shows much closer agreement to the experiment. The insufficient blue shift in the flux-limited model can be explained by a more-diluted corona [see Fig. 122.14(b)],

and, consequently, a deeper location of the light-ray turning points toward the critical radius, where the coronal outflow velocity is reduced.

The structure of the fan tails is less susceptible to the choice of a thermal-transport model but depends more on the presence of CBET. The most-red-shifted parts of the fan tail are produced by light rays that penetrate deeply into the corona, almost reaching the critical-density region. The larger the fraction of the incident light that reaches the critical radius, the more intense the red-shifted spectrum. Such red-shifted fan tails were found in simulations without CBET [Ref. 26, feature B in Fig. 122.18(b)]. In contrast and in agreement with measurements, simulations with CBET predict a less-red-shifted fan tail [Fig. 122.18(c)].

Splitting the incident laser light into two or more colors can reduce the CBET by shifting and suppressing the coupling resonances [Eq. (3)]. This color-splitting technique can be employed to increase the laser absorption in direct-drive implosions. Figure 122.19 shows the predicted variation of the absorption fraction (solid line) for two-color light with a wavelength separation $\Delta\lambda$. Here, the same implosion was assumed as in Fig. 122.16 and the laser energy is equally distributed between the colors. The dashed line in Fig. 122.19 shows the absorption fraction for the model with the expected asymptotic 50% reduction of CBET at $\Delta\lambda \gg \lambda_L(c_a/c)$, which corresponds to $\Delta\lambda = 0$ and η reduced by 0.5 (i.e., $\eta = 0.375$). The increase in the absorption is moderate ($\approx$5%) for $\Delta\lambda \sim 5$ Å and takes the maximum ($\approx$8%) for $\Delta\lambda \sim 8$ to 10 Å. There is
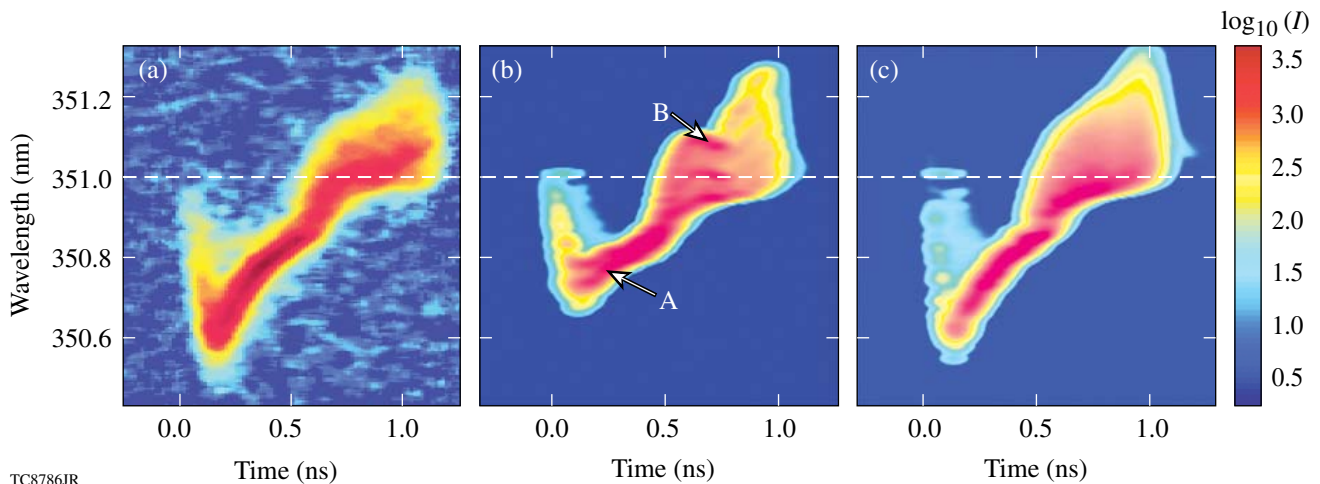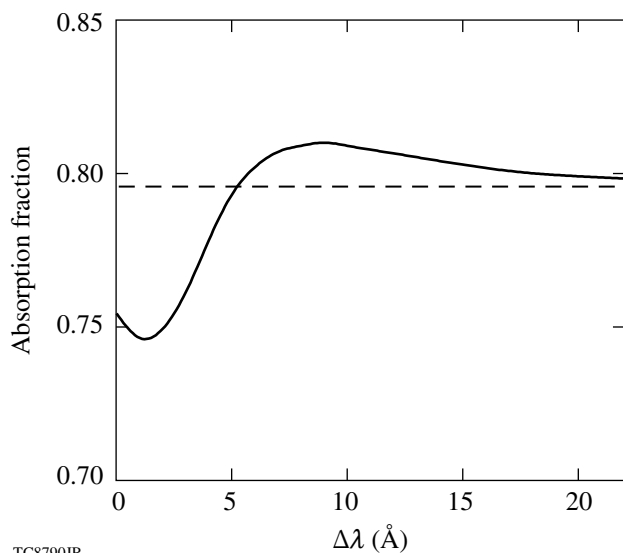

Figure 122.18
(a) Measured and [(b),(c)] simulated scattered-light spectra for a plastic-shell implosion (OMEGA shot 50601). *LILAC* predictions with flux-limited transport are shown in (b), and nonlocal transport with CBET ($\eta = 0.75$) in (c). The laser wavelength is indicated by the dashed lines.

Figure 122.19

Absorption fraction (solid line) as a function of the wavelength separation $\Delta\lambda$ in two-color laser light. The dashed line corresponds to $\Delta\lambda = 0$ and 50%-reduced CBET.

little change in the absorption for $\Delta\lambda < 4$ Å, which confirms the experimental finding that the absorption is insensitive to the use of 1-THz smoothing by special dispersion (SSD),[27] which widens the laser bandwidth by ~3 to 4 Å. It should be noted that this color-splitting technique may be more efficient in direct-drive implosions at the National Ignition Facility[28] because of larger CBET in larger-scale targets.

In summary, it has been shown that the effect of CBET in direct-drive ICF implosions on OMEGA is significant and results in the reduced laser absorption (by ~20% to 30%). *LILAC* simulations using CBET and nonlocal thermal transport show good agreement with bang-time and scattered-light measurements for warm and cryogenic implosions using different pulse shapes and plastic (CH or CD) as an ablator. The simulations, using flux-limited transport ($f = 0.06$) and without CBET, overpredict the absorption for long pulses (>1 ns), resulting in earlier bang-time predictions. The absorption can be increased by employing two-color laser light with a wavelength separation of $\Delta\lambda \sim 5$ to 8 Å.

ACKNOWLEDGMENT

REFERENCES

1. J. D. Lindl, *Inertial Confinement Fusion: The Quest for Ignition and Energy Gain Using Indirect Drive* (Springer-Verlag, New York, 1998), Chap. 6, pp. 39, 61.

2. R. L. McCrory, J. M. Soures, C. P. Verdon, F. J. Marshall, S. A. Letzring, S. Skupsky, T. J. Kessler, R. L. Kremens, J. P. Knauer, H. Kim, J. Delettrez, R. L. Keck, and D. K. Bradley, Nature **335**, 225 (1988).

3. W. L. Kruer, *The Physics of Laser–Plasma Interactions, Frontiers in Physics*, Vol. 73, edited by D. Pines (Addison-Wesley, Redwood City, CA, 1988), Chap. 4, pp. 45, 87.

4. C. J. Randall, J. R. Albritton, and J. J. Thomson, Phys. Fluids **24**, 1474 (1981).

5. J. Myatt, A. V. Maximov, W. Seka, R. S. Craxton, and R. W. Short, Phys. Plasmas **11**, 3394 (2004).

6. W. Seka, H. A. Baldis, J. Fuchs, S. P. Regan, D. D. Meyerhofer, C. Stoeckl, B. Yaakobi, R. S. Craxton, and R. W. Short, Phys. Rev. Lett. **89**, 175002 (2002).

7. T. R. Boehly, D. L. Brown, R. S. Craxton, R. L. Keck, J. P. Knauer, J. H. Kelly, T. J. Kessler, S. A. Kumpan, S. J. Loucks, S. A. Letzring, F. J. Marshall, R. L. McCrory, S. F. B. Morse, W. Seka, J. M. Soures, and C. P. Verdon, Opt. Commun. **133**, 495 (1997).

8. J. Delettrez, R. Epstein, M. C. Richardson, P. A. Jaanimagi, and B. L. Henke, Phys. Rev. A **36**, 3926 (1987).

9. W. Seka, D. H. Edgell, J. P. Knauer, J. F. Myatt, A. V. Maximov, R. W. Short, T. C. Sangster, C. Stoeckl, R. E. Bahr, R. S. Craxton, J. A. Delettrez, V. N. Goncharov, I. V. Igumenshchev, and D. Shvarts, Phys. Plasmas **15**, 056312 (2008).

10. R. A. Lerche, D. W. Phillion, and G. L. Tietbohl, Rev. Sci. Instrum. **66**, 933 (1995).

11. V. N. Goncharov, O. V. Gotchev, E. Vianello, T. R. Boehly, J. P. Knauer, P. W. McKenty, P. B. Radha, S. P. Regan, T. C. Sangster, S. Skupsky, V. A. Smalyuk, R. Betti, R. L. McCrory, D. D. Meyerhofer, and C. Cherfils-Clérouin, Phys. Plasmas **13**, 012702 (2006).

12. V. N. Goncharov, T. C. Sangster, P. B. Radha, R. Betti, T. R. Boehly, T. J. B. Collins, R. S. Craxton, J. A. Delettrez, R. Epstein, V. Yu. Glebov, S. X. Hu, I. V. Igumenshchev, J. P. Knauer, S. J. Loucks, J. A. Marozas, F. J. Marshall, R. L. McCrory, P. W. McKenty, D. D. Meyerhofer, S. P. Regan, W. Seka, S. Skupsky, V. A. Smalyuk, J. M. Soures, C. Stoeckl, D. Shvarts, J. A. Frenje, R. D. Petrasso, C. K. Li, F. Séguin, W. Manheimer, and D. G. Colombant, Phys. Plasmas **15**, 056310 (2008).

13. J. A. F. Hittinger *et al.*, J. Comput. Phys. **209**, 695 (2005).

14. P. Michel *et al.*, Phys. Rev. Lett. **102**, 025004 (2009).

15. T. Dewandre, J. R. Albritton, and E. A. Williams, Phys. Fluids **24**, 528 (1981).

16. E. A. Williams, R. L. Berger, R. P. Drake, A. M. Rubenchik, B. S. Bauer, D. D. Meyerhofer, A. C. Gaeris, and T. W. Johnston, Phys. Plasmas **2**, 129 (1995).

17. A. Shvydky, P. W. McKenty, J. A. Delettrez, I. V. Igumenshchev, D. H. Edgell, S. Skupsky, and R. L. McCrory, Bull. Am. Phys. Soc. **54**, 307 (2009).

18. L. Spitzer, Jr. and R. Härm, Phys. Rev. **89**, 977 (1953).

19. R. C. Malone, R. L. McCrory, and R. L. Morse, Phys. Rev. Lett. **34**, 721 (1975).

20. T. R. Boehly, E. Vianello, J. E. Miller, R. S. Craxton, T. J. B. Collins, V. N. Goncharov, I. V. Igumenshchev, D. D. Meyerhofer, D. G. Hicks, P. M. Celliers, and G. W. Collins, Phys. Plasmas **13**, 056303 (2006).

21. V. N. Goncharov, J. P. Knauer, P. W. McKenty, P. B. Radha, T. C. Sangster, S. Skupsky, R. Betti, R. L. McCrory, and D. D. Meyerhofer, Phys. Plasmas **10**, 1906 (2003).

22. K. Anderson and R. Betti, Phys. Plasmas **11**, 5 (2004).

23. A. Sunahara, J. A. Delettrez, C. Stoeckl, R. W. Short, and S. Skupsky, Phys. Rev. Lett. **91**, 095003 (2003).

24. N. A. Krall and A. W. Trivelpiece, *Principles of Plasma Physics* (San Francisco Press, Inc., San Francisco, 1986), p. 316.

25. I. V. Igumenshchev, V. N. Goncharov, W. Seka, D. Edgell, and T. R. Boehly, Phys. Plasmas **14**, 092701 (2007).

26. D. Edgell, W. Seka, J. A. Delettrez, R. S. Craxton, V. N. Goncharov, I. V. Igumenshchev, J. Myatt, A. V. Maximov, R. W. Short, T. C. Sangster, and R. E. Bahr, Bull. Am. Phys. Soc. **52**, 195 (2007); *ibid*., Bull. Am. Phys. Soc. **53**, 168 (2008); *ibid*., Bull. Am. Phys. Soc. **54**, 145 (2006).

27. S. Skupsky and R. S. Craxton, Phys. Plasmas **6**, 2157 (1999).

28. S. W. Haan, S. M. Pollaine, J. D. Lindl, L. J. Suter, R. L. Berger, L. V. Powers, W. E. Alley, P. A. Amendt, J. A. Futterman, W. K. Levedahl, M. D. Rosen, D. P. Rowley, R. A. Sacks, A. I. Shestakov, G. L. Strobel, M. Tabak, S. V. Weber, G. B. Zimmerman, W. J. Krauser, D. C. Wilson, S. V. Coggeshall, D. B. Harris, N. M. Hoffman, and B. H. Wilde, Phys. Plasmas **2**, 2480 (1995).